Iterative maps with multiple fixed points for excitation of two level systems

H. Cho, J. Baum,[a] and A. Pines
Department of Chemistry, University of California and Materials and Molecular Research Division, Lawrence Berkeley Laboratory, Berkeley, California 94720

(Received 27 October 1986; accepted 5 December 1986)

Iterative schemes have been used in NMR to generate pulse sequences which excite spin systems over narrow or broad ranges of transition frequencies and radio frequency amplitudes. Mathematical methods employing iterative maps and related concepts from nonlinear dynamics have been applied in the analysis of these schemes. The effect of transforming a pulse sequence by an iterative procedure can be represented as an iterative map on a quantum statistical propagator space, with fixed points in this space corresponding to certain desired responses of the spin system. The stability of these points with respect to variations of parameters, such as amplitudes or energies, determines the bandwidth characteristics of the corresponding sequence; broadband behavior results from stable fixed points, and narrowband behavior from unstable fixed points. This paper examines schemes which produce maps with more than one stable fixed point. Such schemes are shown to generate sequences which exhibit bistable or selective, bandpass behavior. Spatially selective NMR, spin decoupling, *nk*-quantum selective multiple-quantum NMR, isotope selective zero-field NMR, and optical information storage are some of the applications which can benefit from bandpass selective excitation sequences.

I. INTRODUCTION

The excitation of specific, well-defined responses is a fundamental and widespread objective of pulsed nuclear magnetic resonance and other types of spectroscopy. Often, this objective must be achieved over a range of experimentally variable parameters and in the presence of experimental constraints, such as limitations on irradiation power. For these cases, a single radio frequency (rf) pulse does not normally suffice to produce the desired response. In an NMR spectrum with several lines, for example, most transitions will not be resonant with the incident rf, precluding the uniform excitation of all lines simultaneously with a single pulse. To counter this fundamental problem, composite pulses, i.e., sequences of time- and phase-modulated pulses which are insensitive to the deficiencies of individual pulses were proposed[1] as replacements for single pulses. In some of the early applications of a composite pulse, it was shown that simple sequences consisting of three or more pulses could uniformly invert the equilibrium populations of isolated two level systems over ranges of resonance frequencies and rf amplitudes considerably broader than those of a single π pulse.[2-15] Composite pulse excitation methods have been fruitfully applied to other problems as well, most notably narrowband excitation,[11,14,16] heteronuclear decoupling in liquids,[17-25] broadband double quantum excitation,[26] uniform excitation of strongly coupled systems,[27,28] coherence transfer between different nuclear spin species,[29] and suppression of homonuclear scalar interactions.[30] An alternative approach employing continuous modulation of phase and frequency related to adiabatic rapid passage and self-induced transparency has been demonstrated by Baum *et al.*[13]

In the great majority of the work on composite pulses, the common motivation has been to modify the effective bandwidth of the response of nuclear spins with respect to some parameter. Broadband inversion sequences, to take a prominent example, maximize the range of transition frequencies or amplitudes over which the rf is effective in inverting populations, while narrowband sequences minimize the effective bandwidths of inversion. For many experiments in NMR, however, more useful sequences are those which can excite a specific, tailored response. The tailoring of a response refers to the selective and uniform excitation of nuclear spins depending on the value of certain specified parameters, e.g., the Larmor frequency ω_0 or the rf amplitude ω_1. In contrast to broadband or narrowband behavior, a tailored response exhibits bandpass behavior.

Bandpass behavior is obtained in NMR when nuclear spins are selectively excited, meaning that some spins in the sample evolve to one final state, and all other spins to a second and distinct final state. Ideally, the final state to which a given spin evolves is determined solely by the value of some experimental parameter λ or set of parameters $\{\lambda\}$. Assuming the two final states are experimentally distinguishable, variations in λ may then be used to discriminate between nuclear spins.

In this paper, we utilize a form of analysis based on iterative maps and their fixed points recently introduced by Tycko *et al.*[11,14] to demonstrate how NMR pulse sequences with bandpass specificity can be generated. This work expands upon results presented in a recent Letter.[31] The sequences we derive here selectively and completely invert resonant isolated spins-1/2 for designated ranges of ω_1, and leave undisturbed from equilibrium all spins which lie outside the selected ω_1 passbands. These kinds of sequences permit the precise discrimination of nuclear spins which differ in some parameter of interest and thus act as spin filters. Experiments in topical NMR, for example, rely on spatially

[a] Present address: Oxford University, South Parks Road, Oxford, OX1 3QR, England.

 0021-9606/87/063089-18$02.10

inhomogeneous rf fields to distinguish between spins in different locations in the sample.[32] In zero field NMR,[33] where the Zeeman energy of nuclear spins is absent, amplitude selective pulse sequences can also be utilized to discriminate between different types of nuclei based on their different gyromagnetic ratios. Other applications of bandwidth specific excitation methods include *nk*-quantum selective multiple quantum NMR,[34–36] and optical information storage.[37]

II. GENERAL THEORY

A. Background

The problem of choosing optimum combinations of pulse phases, frequencies, durations, amplitudes, and spacings for pulse sequences has been the subject of a variety of theoretical treatments in NMR, including average Hamiltonian theory,[38–40] series expansions of rotation operators,[3,4] inverse transform analyses,[41–47] Magnus expansions,[7,12,48] and Bloch vector methods.[49] Although many important sequences have been obtained from these methods, computational complexity typically limits their applicability to sequences with few experimentally variable parameters and small numbers of pulses. This limitation is largely avoided by using an alternative approach which employs iterative schemes to analyze and construct long, highly refined pulse sequences.[9,11,14–25,50] Iterative schemes are algorithms applied repetitively to generate a series of pulse sequence iterates S_0, S_1, S_2, etc. These algorithms are comprised of transformations designed to improve arbitrary pulse sequences with respect to some stated criterion, such as the broadband inversion of spin populations. One possible transformation of a pulse sequence, for example, would be to add some constant amount to the phases of all the pulses. Other transformations which have been proposed include the concatenation of pulses, the cyclic permutation of pulses, and forming the inverse of a sequence. Such iterative schemes in NMR were introduced by Warren *et al.*[50] as a means for obtaining sequences which selectively pumped high order multiple-quantum transitions.

An important feature of this approach is that an iterative procedure is employed to generate iterates which converge to some specifically desired form. The close formal resemblance of this procedure to iterative functions of the type studied in nonlinear dynamics was recognized by Tycko *et al.*,[11] and a comprehensive reformulation of pulse iteration schemes has subsequently been given by them in terms of this formalism.[14] The utility of iterative maps and their fixed points for simulating nonlinear behavior has been well established, and is widely appreciated in many fields outside of NMR.[51,52] In the next section, we provide a short synopsis of some general and useful topics in the theory of iterative maps. After this, we show how these ideas are applied to pulse iteration schemes in NMR, with particular emphasis on the derivation of algorithms which can generate bandpass type sequences. The effect of the initial sequence on the selection of the excitation bandwidth is examined, and a general procedure for tailoring the inversion bandwidths discussed. Finally, a method which takes advantage of the sharp cutoff of the bandpass frequencies is investigated as a way to obtain ω_1 narrowband, phase coherent 90° pulses for use in spatially selective NMR experiments.

B. Review of iterative maps

Generalized definitions for the terminology introduced here can be found in several texts and articles,[51–57] but for the ensuing discussion it will be helpful to briefly review some of the more important concepts. The approaches we take in this paper are based on mathematical methods which employ iterative maps to model nonlinear dynamical processes. The term map will be used here to denote a function which transforms points in some arbitrary space $\mathbf{L}$ to other points in the same space $\mathbf{L}$. A special feature of such functions is that they can be applied iteratively, a property which is summarized by the equation:

$$U_{i+1} = F(U_i). \tag{1}$$

This equation states simply that the $(i+1)$st point is obtained from the ith point by applying the map F. As an example, the ith point may be a pulse sequence, and the map F an iterative scheme.

Fixed points of a map are defined by the equality:

$$\bar{U} = F(\bar{U}). \tag{2}$$

These points are classified according to their stability. The stability of an iterative map refers to the effect the map has on points in the neighborhood of the fixed point. Operationally, a fixed point is considered stable if points in the neighborhood of the fixed point converge to the fixed point upon iteration of the map. For the special case of a map on the one dimensional space $\mathbf{R}^1$, the derivative of the map at stable fixed points obeys the inequality:

$$\left|\frac{dF}{dU}\right|_{U=\bar{U}} < 1. \tag{3}$$

"Superstability" results when this derivative equals zero. The set of points which converge to the fixed point is referred to as the map's basin.

If points in the neighborhood of a fixed point do not converge to the fixed point as the map is iterated, then the fixed point is unstable. This occurs in the case of a one dimensional map when the derivative of the map evaluated at the unstable fixed point satisfies the inequality:

$$\left|\frac{dF}{dU}\right|_{U=\bar{U}} > 1. \tag{4}$$

These definitions can be generalized to a map F on a higher dimensional space by replacing the derivative of the one dimensional map with the eigenvalues of the Jacobian matrix of F evaluated at the fixed points. Since the magnitude of some eigenvalues may be less than one and others greater than one, it is possible for fixed points in a multidimensional space to be stable along some directions but unstable along others. Examples of this kind of behavior are observed in pulse iteration schemes, and will be pointed out later.

An important feature of a one dimensional map with two stable fixed points is depicted in Fig. 1. This figure provides a simple proof that so-called bistable maps must have at least one unstable fixed point between two stable fixed points.[56] The fixed points of a map on $\mathbf{R}^1$ appear as the points

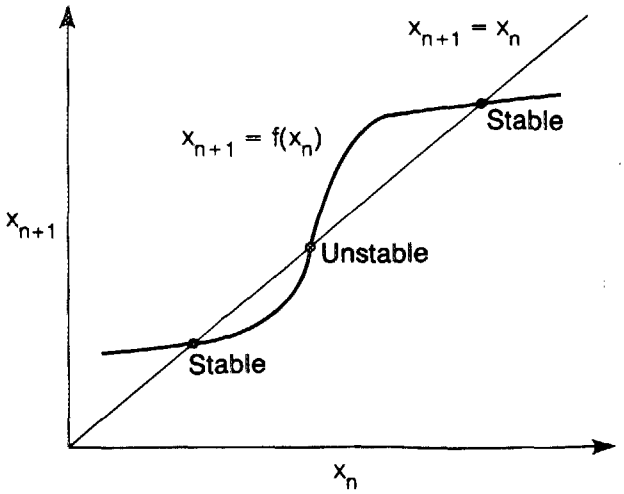

FIG. 1. An example of a one dimensional map with two stable fixed points, appearing as the intersection points of the map with the line $y = x$ with first derivative less than unity. The stability of these two fixed points necessitates the presence of an unstable fixed point intermediate between the two stable points. This point is the intersection point of the map with the $y = x$ line where the first derivative is greater than one.

where the iterative map F intersects the linear function $y = x$. As mentioned earlier, the derivative of F evaluated at stable fixed points is less than unity. The figure shows that between two such points, there must be at least one point where F crosses the $y = x$ line and has derivative greater than unity. From this, it follows that at least one unstable fixed point exists between the two stable fixed points. Note that this does not exclude the possibility of additional fixed points, both stable and unstable, between the two postulated stable fixed points.

The consequences of these results for iterative schemes in bandpass sequences will be discussed in the next section.

C. Applications of iterative maps to spectroscopy

In quantum mechanics, the evolution in time of states and operators is governed by a unitary operator known as the time development operator, or propagator. In its most general form, this operator can be written:

$$U(\lambda,t) = T\exp\left\{-\frac{i}{\hbar}\int_0^t \mathscr{H}(\lambda,t')dt'\right\}, \tag{5}$$

where T is the Dyson time ordering operator and $\mathscr{H}(\lambda,t)$ is the Hamiltonian. The effect of time-dependent perturbations on the state of the system, such as a pulse sequence, is accounted for through the time dependence of the Hamiltonian $\mathscr{H}(\lambda,t)$.

Besides time, the propagator and Hamiltonian can depend on other parameters as well, which we indicate by making U and $\mathscr{H}$ functions of the generic variable λ. In NMR, these parameters might include the rf amplitude ω_1, the resonance frequency, spin coupling constants, or position in space. For a macroscopic NMR sample, these parameters normally assume a range of possible values; there may, for example, be several lines in the spectrum, and therefore several different resonance frequencies. Accordingly, $U(\lambda,t)$ may also assume a range of different values for some time t. NMR experiments, however, usually require a specific propagator $\bar{U}$ in order to bring about some desired final condition. The desired final condition might, e.g., be a population inverted state, in which case the desired $\bar{U}$ would be a π rotation.

A propagator which produces some desired final state is most frequently obtained in NMR with a radio frequency pulse sequence. If the propagator $U(\lambda,t)$ for a pulse sequence is $\bar{U}$ for a wide range of the parameter λ, then the sequence is termed broadband in λ. If the propagator representing the pulse sequence is $\bar{U}$ for only a narrow range of λ values, then the sequence is narrowband with respect to λ. These two cases have already been extensively treated, and many such sequences for different applications have already been proposed. If, however, the propagator for the sequence is $\bar{U}_1$ for some values of λ, and $\bar{U}_2$ for most other values of λ, then we define the sequence as being bistable in λ. This bistability can be exploited to produce bandpass behavior, and it is on this last class of sequences that we shall concentrate in this paper.

The fixed point analysis can be used to address bandwidth excitation problems in the following way. Pulse iteration schemes are rules which transform one pulse sequence S_i into another pulse sequence S_{i+1} with improved, more desirable properties. They may therefore be regarded as maps on propagator space (a subspace of Liouville space) insofar as they transform the propagator $U_i(\lambda,t)$, corresponding to the pulse sequence S_i, to the propagator $U_{i+1}(\lambda,t)$, corresponding to the pulse sequence S_{i+1}, in the manner of Eq. (1). The initial propagator $U_0(\lambda,t)$ may have a range of possible values due to the fact that the parameter λ, on which $U_0(\lambda,t)$ depends, may itself range over a spectrum of values. The object, then, is to obtain $\bar{U}$ from an iterative map given the dependence of propagators on the parameter λ.

In order to create a broadband sequence by using an iterative scheme, the associated iterative map must generate a series of iterates $U_{i+1}(\lambda,t)$ which converge to the desired propagator for a wide range of λ values. To achieve this, the limit of convergence of the map must be insensitive to the choice of the initial condition $U_0(\lambda,t)$. In the language of nonlinear dynamics, $\bar{U}$ is a stable fixed point of the map on propagator space; nearby points converge to $\bar{U}$ as the map is iterated, and $\bar{U}$ is itself invariant upon iteration of the map.

Narrowband sequences on the other hand are generated by maps which are unstable at their fixed points. Because of this instability, the only point which gets mapped to the fixed point $\bar{U}$ is the fixed point itself. The implication then, is that only a very narrow range of parameters result in pulse sequence propagators which get mapped to the unstable fixed point.

D. Mathematical preliminaries

To illustrate these concepts more concretely, we will consider specifically propagators for nuclear spin systems consisting of isolated spins-1/2. The high field rotating frame Hamiltonian for such systems is, in general, a linear function of the spin angular momentum operators I_x, I_y,

and I_z. As a consequence, all possible propagators for this system assume the form:

$$U(t) = \exp\{-i\alpha(\mathbf{r}\cdot\mathbf{I})\}, \quad (6)$$

where $\mathbf{r}$ is a unit vector. Propagators of this form are quantum mechanical rotation operators.

The state of such a system, as described by the density operator formalism, can also be written as a linear function of the spin angular momentum operators, and is therefore specified by a three dimensional vector which we label $\mathbf{M}$. The time behavior of the density operator under the propagator in Eq. (6) can be represented as a rotation of $\mathbf{M}$ about the axis $\mathbf{r}$ through an angle α. This expresses the well-known result that the time evolution of isolated two-level systems, neglecting relaxation, can be rigorously interpreted as the rotation of a three dimensional Cartesian vector, namely, the polarization vector.[49,58]

This result allows us to restrict our attention to the subset of spin propagators which can be described as rotations in three dimensional space. All rotations in this space can be represented by 3×3 real orthogonal matrices with determinant equal to unity.[59–61] This set of rotations forms the group $SO(3)$, pictured in Fig. 2 as a solid sphere of radius π. A rotation is uniquely defined in this representation by a unit vector drawn from the origin, denoting the axis of the rotation, and a distance from the origin, denoting the angle of the rotation. The axis and angle may be identified in Eq. (6) as $\mathbf{r}$ and α, respectively.

Adopting the notation of Ref. 14, an element in $SO(3)$ describing a rotation about an angle α around one of the three orthogonal axes x, y, or z will be written as $R_x(\alpha)$, $R_y(\alpha)$, or $R_z(\alpha)$, respectively. A rotation about an axis in the xy plane of $SO(3)$ making an angle ϕ with the x axis will appear as $R_\phi(\alpha)$. A generalized rotation around an axis $\mathbf{r}$ about an angle α will be represented as $R(\alpha)$. For the sake of expedience, we will work exclusively with $SO(3)$ and perform all calculations in this representation, and regard time evolution operators of the spin system as rotation operators.

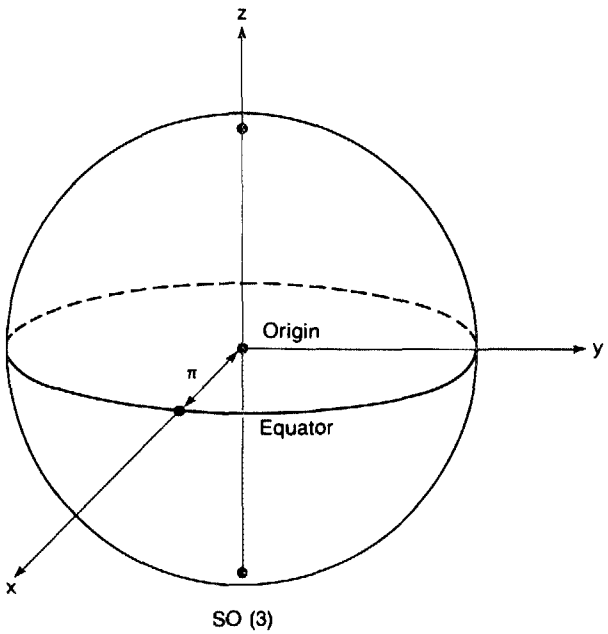

FIG. 2. Graphic representation of the real three dimensional space of rotations $SO(3)$ as a sphere of radius π. Rotations are represented as vectors in this space, with the direction of the vector defining the axis of the rotation and the norm of the vector defining the angle of the rotation.

E. Flow diagrams

The set of rotations commonly referred to as π or inversion pulses appears in Fig. 2 as the circumference of the sphere in the xy plane, known as the equator. This set contains all rotations which take $+z$ to $-z$. The identity operator is represented on this picture by the origin.

Broadband inversion sequences for uncoupled spins are generated from iterative maps in $SO(3)$ which have the equator as a stable fixed set. For an initial point $R(\alpha_0)$ in the neighborhood of the equator, such maps generate a series of iterates $R(\alpha_i)$ which converge to the equator, that is, to a π rotation. The convergence to the equator of points in the neighborhood of the equator is depicted in Fig. 3(a). This figure shows an xy cross section of $SO(3)$. A second fixed point of this hypothetical map is the origin, shown here as an unstable fixed point. The arrows indicate the direction in which points in this plane move, away from the origin and towards the equator, when the map is iterated. This motion is called the flow of the map.[54–57] It should be noted here that this map is atypical in the sense that it shows points in the xy plane being mapped only to other points in the same plane. In general, a map on $SO(3)$ will not behave in this way. Special cases of maps which do have this property play an important role in the future discussion, however, and will be examined presently.

Figure 3(b) illustrates the flow of points in the xy plane of $SO(3)$ for maps which produce narrowband π pulse sequences. Here, the equator and origin are fixed points as for the broadband case. The direction of the flow, though, has been reversed; it is now the equator which is unstable and the origin which is stable. The equator is fixed so that if $R(\bar{\alpha})$ is a point on the equator, i.e., is a π rotation, then $F[R(\bar{\alpha})]$ will remain a π rotation. All other points on this plane, however, converge to the origin, becoming identity operations. The result is a sequence which inverts spins over a narrow range of some parameter λ, and does not affect spins which lie outside this narrow range.

The flow of points for a map that produces a square, or bistable, inversion sequence is shown in Fig. 3(c). This map has the origin and the equator as fixed sets, but in contrast to the two previous cases, both, instead of one, of the fixed sets are stable. A significant consequence of this bistability is the presence of an unstable fixed circle in the xy plane between the origin and the equator. In Sec. II B, the necessity of an unstable fixed point between two stable fixed points for a one dimensional map was demonstrated. This result does not generally apply to maps on $SO(3)$, since $SO(3)$ is not a one dimensional space. The particular map shown here is exceptional, however, because it maps points on the xy plane only to points also on the xy plane. It will be shown in the next section that if we ignore the rotation around the z axis produced by the map, then a map on $SO(3)$ with this property

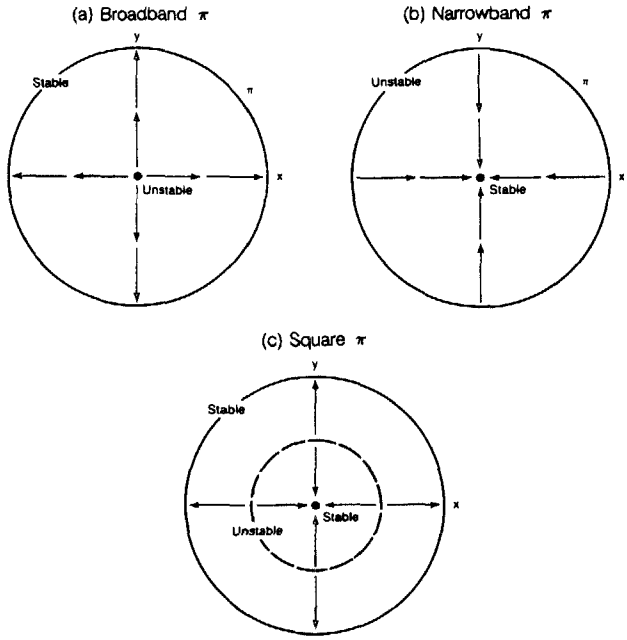

FIG. 3. Cross section of the xy plane of $SO(3)$ illustrating the flow of maps for (a) broadband, (b) narrowband, and (c) bandpass iterative schemes. The arrows indicate symbolically the direction in which points on this plane move when operated on by the various maps, towards stable fixed points and away from unstable fixed points.

can be considered fundamentally one dimensional. Given this, the bistability theorem introduced in the previous section becomes applicable to the present case.

The bistability of the map in Fig. 3(c) is evidenced by the opposing arrows showing convergence to two fixed sets, viz., the equator and the origin. The existence of the third unstable fixed set is required by the continuity of the map, and will be examined more thoroughly later on. This figure suggests that on this plane, three distinct classes of points exist. First are the points within the unstable fixed circle; these points move towards the origin as the map is iterated. Second is the unstable fixed circle itself, which, by definition, remains invariant, and to which no other points converge. The third class is the set of points which lie outside the unstable fixed circle and converge to the equator as the map is applied.

The effect of applying the map is to move points closer to the origin or the equator depending on whether the initial point $R(\alpha_0)$ is inside or outside the unstable fixed circle. This movement to one of two stable fixed sets of propagators essentially is the origin of the bistable bandpass response.

The preceding sections have established the following ideas. Pulse iteration schemes transform a pulse sequence S_i to S_{i+1} Associated with this transformation of pulse sequences is a transformation of the propagator U_i to the propagator U_{i+1}. This transformation is a map on the propagator space. To obtain a desired propagator $\bar{U}$ from a pulse sequence with an iterative scheme, the iterative scheme must have a corresponding map on the space which has $\bar{U}$ as a fixed point. The stability of the map in various directions determines the bandwidth properties of the sequence. Sequences which excite a bandpass response may be obtained from iterative maps with two stable fixed points. A bistable map causes most points to converge to either one of the two desired propagators $\bar{U}_1$ or $\bar{U}_2$ depending on the value of some parameter λ, and thereby produces the bandpass response. This idea is demonstrated here for maps which have the equator and the origin of $SO(3)$ as the two stable fixed sets. Iteration of the map results in the convergence of propagators to the two stable fixed points associated with the two possible responses of the spin system to the rf radiation. Experimentally, these propagators represent sequences which selectively invert nuclear spins depending on the rf amplitude at the spin's position.

III. DERIVATION OF ITERATIVE SCHEMES

A. Iterative schemes and maps on $SO(3)$

The pulse iteration schemes we shall develop in this section are comprised of two basic operations. These will be demonstrated schematically on an arbitrary pulse sequence which we designate S_i. The schemes we seek are those defining maps on $SO(3)$ with the equator and the origin as stable fixed sets and the xy plane as an invariant set of the map.

The first operation consists of forming phase shifted versions of S_i. We perform this transformation by adding some constant amount ϕ_k to the phase of each pulse in S_i. The pulse sequence thus transformed will be denoted $S_i(\phi_k)$. The phase index k ranges from 1 to N, where N is the number of different phase shifts to be performed.

The second operation is to concatenate the N phase shifted versions of S_i. The result will be a sequence N times longer than S_i. The new sequence, S_{i+1}, will be

$$S_{i+1} = S_i(\phi_1)S_i(\phi_2)\cdots S_i(\phi_{N-1})S_i(\phi_N). \tag{7}$$

Clearly, both operations can be applied repetitively on any starting sequence. The notation which has been adopted to summarize the combination of these two operations is $[\phi_1, \phi_2, \phi_3,\ldots,\phi_N]$. The uniquely defined rotation operator corresponding to S_i can be expressed similarly in the form:

$$R(\alpha_{i+1}) = R(\alpha_{i,N})R(\alpha_{i,N-1})\cdots R(\alpha_{i,2})R(\alpha_{i,1}), \tag{8}$$

where $\alpha_{i,j}$ equals the vector $\alpha_i[\sin\theta_i\cos(\phi_i+\phi_j), \sin\theta_i\sin(\phi_i+\phi_j), \cos\theta_i]$ and $R(\alpha_{i,j}) = R_z(\phi_j)R(\alpha_i)R_z^{-1}(\phi_j)$. Here, θ_i and ϕ_i are the usual polar and azimuthal angles of a spherical polar coordinate system. Because of the group property of rotations, the product of rotation operators on the right always equals a rotation operator.

By limiting ourselves to these two operations, we have reduced the problem of designing a pulse iteration scheme to a matter of selecting the N phases $\phi_1, \phi_2, \phi_3,\ldots, \phi_N$. In choosing these phases, we will observe two constraints. The first is that we will require N to be an odd number. This constraint insures that the equator of $SO(3)$ will be a fixed set of the map associated with this pulse iteration scheme. This assertion follows from the fact that concatenating an odd number of inversion sequences results in an inversion sequence. The necessity of making the equator a fixed set was discussed previously. No such restriction is required in this case to make the origin a fixed point since the origin is always a fixed

point for any mapping derived from a simple phase shift scheme.

The second constraint we impose will be to demand that the phase shift scheme be symmetric. A symmetric phase shift scheme is one for which $\phi_i = \phi_{N-i+1}$, e.g., $\phi_1 = \phi_N$, $\phi_2 = \phi_{N-1}$, etc. This last constraint deserves special comment. In the preceding section, it was noted that maps on $SO(3)$ usually do not transform points on the xy plane only to other points on the xy plane. Symmetric phase shift schemes provide a convenient way to obtain maps with this property. Schemes for which the rf amplitude $\omega_1(t)$ and phase $\phi(t)$ are symmetric functions of time have corresponding maps which transform points on the xy plane only to other points in this same plane, hence making this plane an invariant set. A formal proof of this assertion and associated symmetry related properties has been discussed in Ref. 14.

B. One dimensional maps on $SO(3)$

A single pulse produces a rotation around an axis in the xy plane provided the radio frequency irradiation is exactly resonant with the transition frequency. This is evident from considering the rotating frame Hamiltonian during irradiation (in angular frequency units):

$$\mathcal{H} = \omega_1(I_x \cos\phi + I_y \sin\phi) + \Delta\omega I_z \tag{9}$$

which results in the propagator

$$U(t) = \exp\{-i\hbar^{-1}[\omega_1(I_x \cos\phi + I_y \sin\phi) + \Delta\omega I_z]t\}, \tag{10}$$

where ϕ is the phase of the pulse, $\Delta\omega$ is the resonance offset, and t is the duration of the pulse. The unnormalized axis of rotation is given by the vector $(\omega_1 \cos\phi, \omega_1 \sin\phi, \Delta\omega)$, and lies in the xy plane if and only if $\Delta\omega$ is zero.

Let us consider now a general pulse sequence S_i which produces as its net effect on the density operator a rotation around an axis in the xy plane. The rotation operator corresponding to S_i can be written as $R(\alpha_i)$, where α_i is the vector

$$\alpha_i = \alpha_i(\cos\phi_i, \sin\phi_i, 0). \tag{11}$$

Again, α_i is the angle and $(\cos\phi_i, \sin\phi_i, 0)$ the normalized axis of the rotation. The phase symmetry theorem states that if S_i is transformed according to a phase shift algorithm which is symmetric, the new rotation operator corresponding to the transformed sequence S_{i+1} must be of the form $R(\alpha_{i+1})$, where

$$\alpha_{i+1} = \alpha_{i+1}(\cos\phi_{i+1}, \sin\phi_{i+1}, 0). \tag{12}$$

The map $F[R(\alpha_i)] = R(\alpha_{i+1})$ corresponding to a phase shift-concatenation operation is a well defined function on $SO(3)$. This point is made clear by Eq. (8). For a function which maps points on the xy plane only to other points on the xy plane, this implies that α_{i+1} and ϕ_{i+1} are determined uniquely by α_i and ϕ_i. In fact, for such maps, α_{i+1} is specified solely by α_i, as can be seen from the following considerations.

Assume S_i' is a pulse sequence related to the pulse sequence S_i by a constant phase shift of all the pulses $\Delta\phi$. The rotation operator for S_i', $R(\alpha_i')$, is related to the operator $R(\alpha_i)$ by the similarity transformation:

$$R(\alpha_i) = R_z(\Delta\phi)R(\alpha_i')R_z^{-1}(\Delta\phi). \tag{13}$$

Now if we apply a phase shift scheme $[\phi_1, \phi_2, \phi_3, \ldots, \phi_N]$ to S_i and S_i' to form S_{i+1} and S_{i+1}', it follows after some algebra [cf. Eq. (8)] that $R(\alpha_{i+1})$ and $R(\alpha_{i+1}')$ are related by

$$R(\alpha_{i+1}) = R_z(\Delta\phi)R(\alpha_{i+1}')R_z^{-1}(\Delta\phi). \tag{14}$$

Since $\Delta\phi$ is arbitrary, we conclude from this equality that for any map on $SO(3)$ derived from a phase shift scheme, α_{i+1} is independent of ϕ_i.

If the initial iterate, $R(\alpha_0)$, is a point in the xy plane of $SO(3)$ and the map a function derived from a symmetric phase shift scheme, this result, combined with Eq. (11), imply that the only variable determining α_{i+1} will be α_i, i.e.,

$$\alpha_{i+1} = f_s(\alpha_i). \tag{15}$$

Comparison of this expression with Eq. (1) reveals that Eq. (15) defines a one dimensional map in α. This map can have fixed points $\bar{\alpha}$, although what we call fixed points of f_s correspond to, in actuality, fixed circles of radius $\bar{\alpha}$ in the xy plane of $SO(3)$. The two fixed circles of particular concern to us here are the equator and the origin, defined by the set $\{\bar{R}\}$ such that

$$\bar{R} = R_\phi(\bar{\alpha}), \tag{16}$$

where $0 \leqslant \phi \leqslant 2\pi$, and $\bar{\alpha} = 0$ for the origin and $\bar{\alpha} = \pi$ for the equator.

Because points in $SO(3)$ are specified by three coordinates, maps on this space are generally three dimensional functions. Consequently, such maps must normally be analyzed for stability at their fixed points along three orthogonal directions. Equation (15) suggests, however, that under a special set of conditions, discussed earlier, this three dimensional problem can be reduced to one dimension.

The simplification of this problem to one dimension now permits the application of the one dimensional bistability theorem stated in Sec. II B. The values of α we seek to make fixed and stable points of the map in Eq. (15) are $\bar{\alpha}_1 = 0$ and $\bar{\alpha}_2 = \pi$. Stability at these fixed points, by the bistability theorem, necessitates the existence of a third fixed point $\bar{\alpha}_{\text{unstable}}$ lying in the range $\bar{\alpha}_1 < \bar{\alpha}_{\text{unstable}} < \bar{\alpha}_2$, which is unstable. As for $\bar{\alpha}_1$ and $\bar{\alpha}_2$, $\bar{\alpha}_{\text{unstable}}$ defines a circle in the xy plane of $SO(3)$. Points within the range $\bar{\alpha}_1 \leqslant \alpha < \bar{\alpha}_{\text{unstable}}$ move away from $\bar{\alpha}_{\text{unstable}}$ and towards $\bar{\alpha}_1$ as the mapping is repeated, becoming identity operators. Points in the range $\bar{\alpha}_{\text{unstable}} < \alpha \leqslant \bar{\alpha}_2$ also move away from $\bar{\alpha}_{\text{unstable}}$ but towards $\bar{\alpha}_2$ as the mapping is iterated becoming, instead, π rotations. This flow of points was described in Sec. II E, and is depicted in Fig. 3. In such a way, all points in the xy plane not on the unstable circle eventually get mapped, in some well-defined fashion, to one of two possible sets of points, the identity operator or a π rotation.

C. Specification of stability

The invariance of the equator and the origin of $SO(3)$ is guaranteed for a map corresponding to a phase iteration scheme, provided the scheme obeys the constraints set forth in the previous sections. The present discussion will be devoted to maps which, in addition to this invariance, are stable at these two points.

To begin, we examine methods for specifying the stability of a map at each of these points individually. These methods have already been considered in detail elsewhere,[14] and so will be presented only in outline form here.

Points in the neighborhood of the origin are those operators $R(\alpha_i)$ for which $|\alpha_i|$ is small. If an iterative map derived from a phase shift scheme acts on a rotation operator satisfying this condition, the next iterate, given analytically by Eq. (8), is well approximated by the linearized expression:

$$R(\alpha_{i+1}) \approx R\left(\sum_{j=1}^{N} \alpha_{i,j}\right), \tag{17}$$

where $\alpha_{i,j}$ is defined as in Eq. (8). The argument of the term on the right is related to α_i by a simple linear transformation, which we denote $T^{(\text{origin})}$. This linear transformation has eigenvalues N and $\lambda_0^{\pm}$, where

$$\lambda_0^{\pm} = \sum_{j=1}^{N} \exp(\pm i\phi_j). \tag{18}$$

Convergence to the fixed origin is indicated when $|\alpha_i| > |\alpha_{i+1}|$. For displacements in the xy plane, this occurs when two of the eigenvalues of $T^{(\text{origin})}$, $\lambda_0^{\pm}$, are less than one. The possibility of course exists that only one of these eigenvalues is less than one. In such a case, convergence would occur only in certain directions, specifically, those directions parallel to the eigenvector of the stable eigenvalue. The flow of points in the xy plane produced by a map with a stable origin has been shown in Fig. 3(b).

The analysis of convergence to the equator requires a more involved approach. We proceed by first performing the completely general decomposition of a rotation $R(\alpha_i)$ into the product rotation:

$$R(\alpha_i) = R_{\phi_i}(\pi) R(\epsilon_i), \tag{19}$$

where $\epsilon = (\epsilon_x, \epsilon_y, 0)$. Points close to the equator have small $|\epsilon_i|$. Applying an iterative function to this product rotation in the manner of Eq. (8), the next iterate $R(\alpha_{i+1})$ can be shown in the linear approximation to equal

$$R(\alpha_{i+1}) = R_{\phi_i+\gamma}(\pi) R(\epsilon_{i+1}). \tag{20}$$

To compare the rotation $R(\alpha_{i+1})$ with $R(\alpha_i)$ for convergence to the equator, it is necessary to rotate $R(\alpha_{i+1})$ so that the main part of $R(\alpha_{i+1})$, $R_{\phi_i+\gamma}(\pi)$, is coincident with the main part of $R(\alpha_i)$, $R_{\phi_i}(\pi)$. This reflects the fact that the overall z rotation produced by the mapping, corresponding to a phase shift by γ of the rotation axis, is irrelevant when determining convergence to a fixed circle in the xy plane, e.g., the equator.

Performing this transformation on $R(\alpha_{i+1})$ yields the rotation $R_{\phi_i}(\pi) R(\epsilon'_{i+1})$. The argument ϵ'_{i+1} can be expressed as a linear transformation of ϵ_i with eigenvalues:

$$\begin{aligned}\lambda_e^{\pm} = {} & (\cos\Gamma'_1 + \cos\Gamma'_3 + \cdots + \cos\Gamma'_N) \\ & \pm \big[(\cos\Gamma'_2 + \cos\Gamma'_4 + \cdots + \cos\Gamma'_{N-1})^2 \\ & + (\sin\Gamma'_2 + \sin\Gamma'_4 + \cdots + \sin\Gamma'_{N-1})^2 \\ & - (\sin\Gamma'_1 + \sin\Gamma'_3 + \cdots + \sin\Gamma'_N)^2\big]^{1/2},\end{aligned} \tag{21a}$$

where

$$\Gamma'_n = \Gamma_n + (-1)^n \phi_T, \tag{21b}$$

$$\phi_T = \phi_1 - \phi_2 + \cdots - \phi_{N-1} + \phi_N, \tag{21c}$$

$$\Gamma_n = \begin{cases} \phi_n + \sum_{m=1}^{n-1} (-1)^{m+1} 2\phi_m, & n \text{ odd} \\ \phi_n - 2\gamma + \sum_{m=1}^{n-1} (-1)^m 2\phi_m, & n \text{ even} \end{cases}. \tag{21d}$$

As in the case of the origin, these eigenvalues indicate stability for the map along directions coincident with the corresponding eigenvectors when their magnitudes are less than one. The flow in the xy plane expected from a map stable at the equator appears in Fig. 3(a).

D. Bistability in phase symmetric schemes

The four eigenvalue equations in Eqs. (18) and (21) suggest that obtaining stability at the equator and the origin requires that four inequalities be simultaneously satisfied, namely,

$$|\lambda_0^{\pm}| < 1, \tag{22a}$$

$$|\lambda_e^{\pm}| < 1. \tag{22b}$$

The analysis of Sec. III A has proven, however, that the iterative function underlying the map on $SO(3)$ is single dimensional. For the one dimensional case, specifying stability at two fixed points entails satisfying only two inequalities. From this, we conclude that requiring all four inequalities above overdetermines the stability we seek, and that it suffices to meet only two of these inequalities, one at the origin and one at the equator.

Although satisfying these two inequalities assures the stability of a map, the maps we present in this section actually fulfill a more rigorous condition at the two fixed points, that of superstability. Superstability in this space is obtained when the eigenvalues equal zero, and hence involves solving the two nonlinear equations

$$|\lambda_e^{\pm}| = 0, \tag{23a}$$

$$|\lambda_0^{+}| = 0. \tag{23b}$$

The independent variables in these equations are the phase shifts ϕ_i of the scheme. The choice of phase shifts is constrained by the criteria enumerated in Sec. III A. With these constraints, the number of free parameters available to solve these equations is $(N-1)/2$, where N, the number of phases in the sequence, is odd for reasons explained previously.

Solutions to these two equations were determined numerically on a computer using a steepest descent root-finding procedure.[62] One such solution to a good approximation leads to the phase shift scheme:

$$[0, 270, 120, 165, 120, 270, 0]. \tag{A}$$

A second phase shift scheme was calculated similarly, but which additionally satisfies the superstability condition for both eigenvalue equations at the equator [see Eq. (21)]. Solving this extra equation required one additional parameter, with the result that a nine shift scheme was produced:

$$[0, 15, 180, 165, 270, 165, 180, 15, 0]. \tag{B}$$

IV. PROPERTIES OF BISTABLE ITERATIVE SCHEMES

A. Convergence properties of the seven and nine shift sequences: Basin images

Both phase shift algorithms proposed above fulfill the criteria stated earlier for invariance and stability at the equator and the origin of $SO(3)$, and hence both produce the flow of points in the xy plane described in Fig. 3. This fact is confirmed by the xy basin images[14] of the two maps displayed in Figs. 4(a) and 4(b). The basin of a fixed point for some map is defined to be the set of points which converge to the fixed point upon transformation by the map. The images in Figs. 4(a) and 4(b) show the basins in the xy plane of $SO(3)$ for the two bistable maps. The shade at a point on this plane is a measure of the number of iterations of the scheme necessary for the point to converge to one of the two stable fixed points—the lighter the shade, the fewer the number of iterations required. The gray scale to the left gives the actual correspondence between the shade and the number of iterations. Convergence for the ith iterate was decided when $|180 - \alpha_i| \leqslant 5°$ at the equator, and $|\alpha_i| \leqslant 5°$ at the origin.

Several features are immediately apparent in these images. In their gross features, both images are extremely similar. Both basins possess an axial symmetry about the z axis, corroborating a conclusion drawn in Sec. III A, i.e., that maps derived from phase shift schemes are independent of the azimuthal angle coordinate ϕ of a point in $SO(3)$. In the xy plane, the only relevant quantity in determining the convergence of a point to one of the fixed sets is α, the distance of the point from the origin.

The lightest areas in these images appear near the equator and in the circular region centered at the origin. These correspond to the loci of points which are mapped after only a few iterations to the nearby stable fixed point, i.e., the equator or the origin. For both images, the basin of the equator is separated from the basin of the origin by a thin, distinct dark circle. This intermediate circle is the unstable fixed set whose existence, as we saw earlier, is necessitated by the bistability of the one dimensional map. Within this circle, all points converge to the origin, most after a relatively small number of iterations. Outside this unstable fixed circle, no points converge to the origin.

Similar behavior is observed within the basin of the equator. The equator's basin consists of a hollow ring, bounded on the interior by the unstable fixed circle. Outside this circle, all points converge to the equator, becoming π rotations. The bidirectional flow we observe in these figures verifies the flow hypothesized in Fig. 3(c).

A different perspective on the flow of points is offered by Figs. 5 and 6. These figures show the actual movement in the

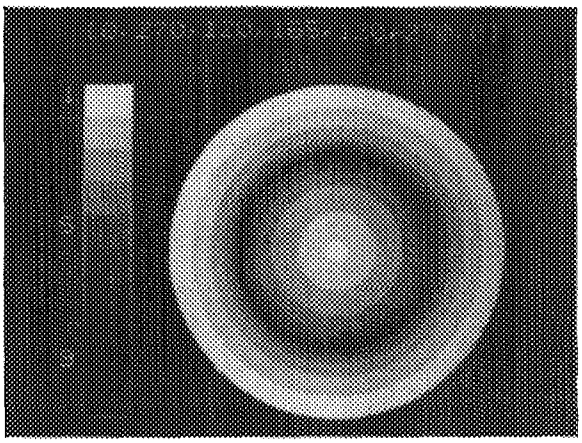

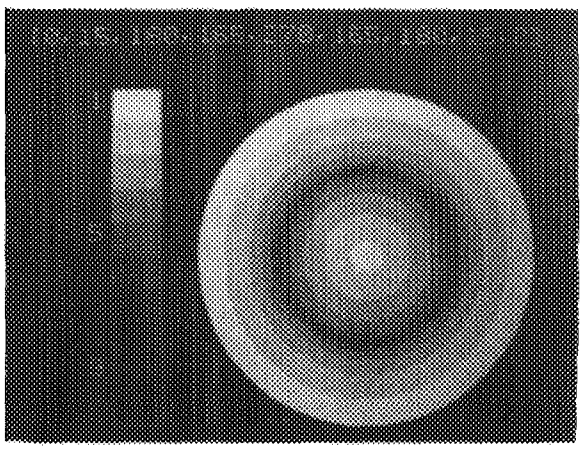

FIG. 4. Basins in the xy plane of $SO(3)$ for (a) the map of the scheme [0, 270, 120, 165, 120, 270, 0] and (b) the map of the scheme [0, 15, 180, 165, 270, 165, 180, 15, 0]. The basin appears as the light colored regions and identifies points which converge to a fixed point after iteration of the map. The gray scale to the left reveals the correspondence of the shade to the number of iterations required for convergence. The presence of two stable fixed points is manifested in both by the presence of large basins around the equator and the origin.

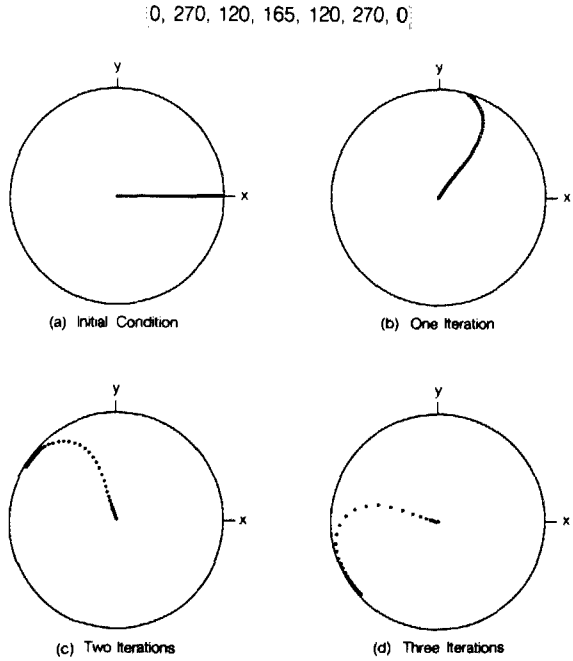

FIG. 5. Displacement of points in the xy plane as a result of being transformed by the map of the scheme [0, 270, 120, 165, 120, 270, 0]. In (a) is the initial set of points $R(\alpha_0)$. Applying the map once to these points results in a displacement to the set of points in (b), twice, in the set of points in (c), and three times in the points in (d). This figure reveals the expected movement of points both towards the equator and towards the origin.

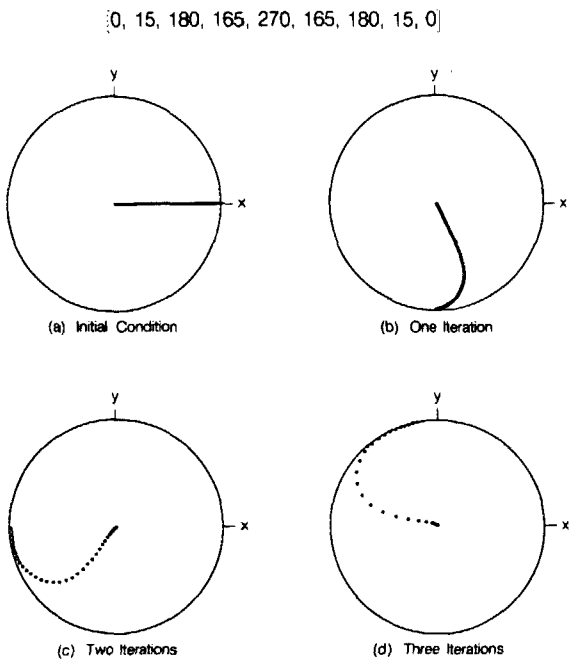

FIG. 6. A version of Fig. 5 for the scheme [0, 15, 180, 165, 270, 165, 180, 15, 0].

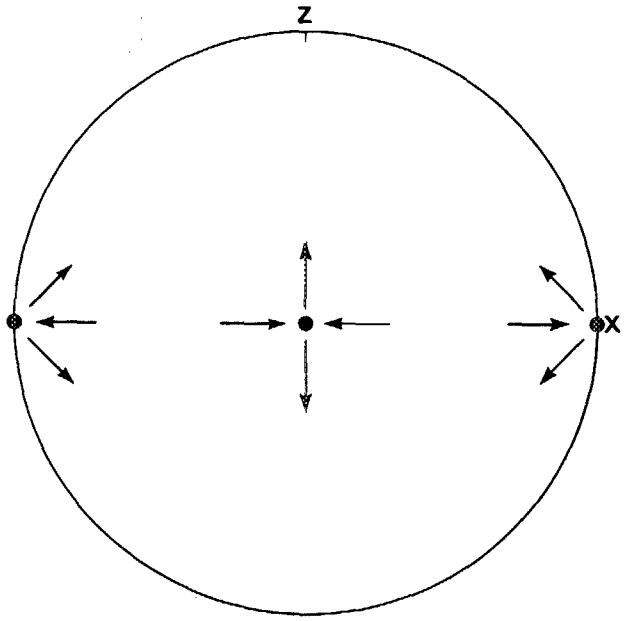

FIG. 7. Flow in a plane of $SO(3)$ containing the z axis for a map which is stable at the origin and the equator only for displacements in the xy plane. Points lying out of this plane move away from these two fixed sets when transformed by the map. The stable directions are given by the eigenvectors of the Jacobian of the map with eigenvalues less than one. The flow expected for such a map is depicted here.

xy plane of an initial set of points from one iteration to the next. The bidirectional flow of points to the equator and origin depending on their distance from the origin is evident in these pictures, with points in between becoming sparser for increasing iterations.

The analysis of these two schemes thus far has not revealed any substantive differences between them. Qualitatively, both have similar flow properties in the xy plane leading to the desired bistable response. Indeed, the distinction between them is not apparent unless we examine the behavior of the map for points off the xy plane. This distinction is illustrated by Figs. 7 and 8. The arrows in Fig. 7 indicate the stability of the origin and the equator for the seven shift scheme along directions lying in the xy plane and the instability of points along directions not in this plane. This instability is symbolized by the arrows pointing outward, away from the origin and the equator in the z direction.

Figure 8 is a schematic flow diagram for the map corresponding to the nine shift scheme. In the xy plane, the bidirectional flow properties are similar to the seven shift scheme, as we have seen earlier. In contrast to Fig. 7, however, all arrows at the equator point in towards the equator, including those out of the xy plane. The implication here is that the mapping for the nine pulse scheme is stable in all directions at the equator.

These observations are substantiated by the basin images in Fig. 9 showing cross sections of $SO(3)$ containing the z axis. Again, because of axial symmetry, all such z cross sections are identical. As in the xy basin images displayed earlier, these images depict the superposition of the basins of both the equator and the origin. The basin image for the seven shift scheme, while showing some regions out of the xy plane which are convergent to one of the fixed points, nevertheless is mostly black, indicating that most points in $SO(3)$ do not converge to either fixed point. The nine shift scheme on the other hand generates an image which shows a large portion of the space converging to the equator because of the additional direction of stability of this point. Like basin images reported earlier of broadband sequences, this image has a self-similar fractal structure.[63]

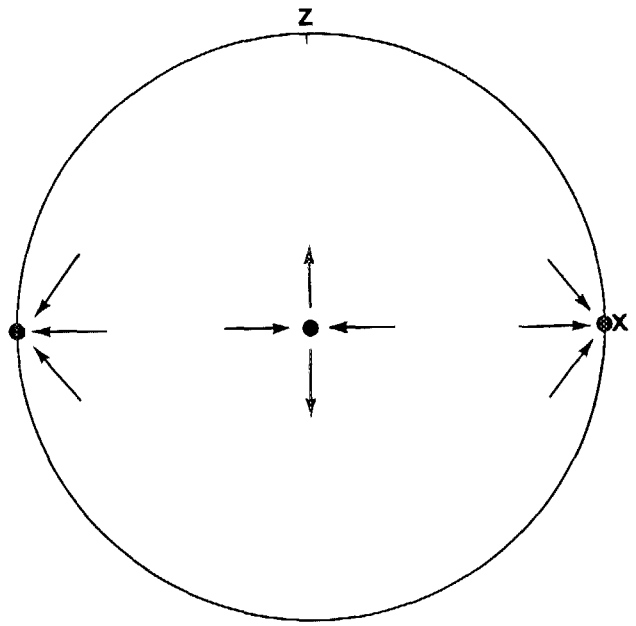

FIG. 8. Same as Fig. 7, but for a map which is stable in all directions at the equator. All arrows are now shown pointing in towards the equator denoting this flow.

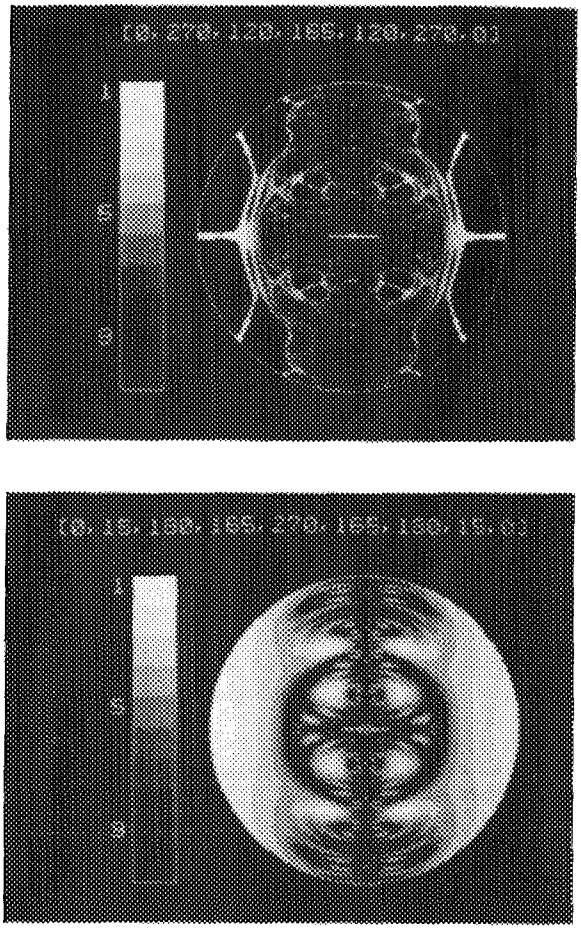

FIG. 9. Basin images for the schemes (a) [0, 270, 120, 165, 120, 270, 0] and (b) [0, 15, 180, 165, 270, 165, 180, 15, 0] showing a cross section of $SO(3)$ containing the z axis. The size and shape of the basin in (b), particularly near the equator, manifests the stability in all directions of the fixed equator. The basin image in (a), on the other hand, shows a smaller basin, indicating the instability of the equator in directions with a z component. Notable also are the thin bright horizontal lines in both, centered at the origin, denoting the basin of the origin which lies in the xy plane.

The reason for the differences between the basin images can be understood by recalling the derivation of these algorithms in Sec. III B. Four inequalities were derived in this section as necessary criteria for determining the stability of the equator and origin, two at both points. For specifying stability at the equator and origin with respect to displacements in the xy plane, it was found sufficient to satisfy only two of these inequalities. The seven shift scheme does, in fact, satisfy these two inequalities, and therefore is stable only for displacements in the xy plane. The nine shift scheme, however, satisfies the inequalities for both, rather than one, eigenvalues at the equator. Consequently, the nine shift scheme has an additional direction of stability at the equator that the seven shift scheme does not possess. This added direction is given by the eigenvector of the second stable eigenvalue, and is the origin of the extra stability in the z direction of the mapping for the nine shift scheme. This means the nine shift map is stable with respect to frequency offset at the equator, i.e., for π rotations.

B. Bandwidth properties of bistable schemes

Producing specific pulse sequences with schemes (A) and (B) requires that an initial sequence be specified. The simplest initial sequence to consider is the case of a single resonant pulse. Applying the seven shift scheme (A) to this initial condition generates sequences consisting of 7^n pulses, where n is the number of times the scheme is iterated. According to the analysis given earlier, the propagators for these higher iterate sequences will converge either to the identity operator or an inversion operator. The parameter determining this limit of convergence for some initial iterate $R(\alpha_0)$ is α_0, the initial angle of rotation.

For a single, resonant pulse of fixed duration t_p, α_0 is equal to $\omega_1 t_p$. From this relationship, we draw the conclusion that the limit to which the higher iterate propagators converges depends solely on the value of ω_1. If ω_1 is small enough so that $\omega_1 t_p < \bar{\alpha}_{\text{unstable}}$, then the higher iterate propagators converge to the identity operator. If $\omega_1 t_p > \bar{\alpha}_{\text{unstable}}$, then the iterates converge to an inverting rotation as the scheme is iterated. More generally, the propagator U_0 for a single pulse converges to an inversion operation for rf amplitudes lying in the range:

$$\bar{\alpha}_{\text{unstable}} < \omega_1 t_p \bmod 2\pi < 2\pi - \bar{\alpha}_{\text{unstable}}. \tag{24}$$

Outside these ranges, the limit of convergence is the identity operator. Similar results hold for the nine shift scheme.

Exact theoretical simulations of the inversion performance of these sequences as a function of ω_1 are presented in Figs. 10 and 11. Formally, the inversion is defined as the projection of the spin density operator after the pulse sequence onto the operator I_z, which can be found from the equation:

$$\langle I_z \rangle = \mathrm{Tr}\{I_z U(t) I_z U^\dagger(t)\}/\mathrm{Tr}\{I_z^2\}. \tag{25}$$

In both figures are three curves, showing the inversion for a single pulse, one iteration of the scheme on a single

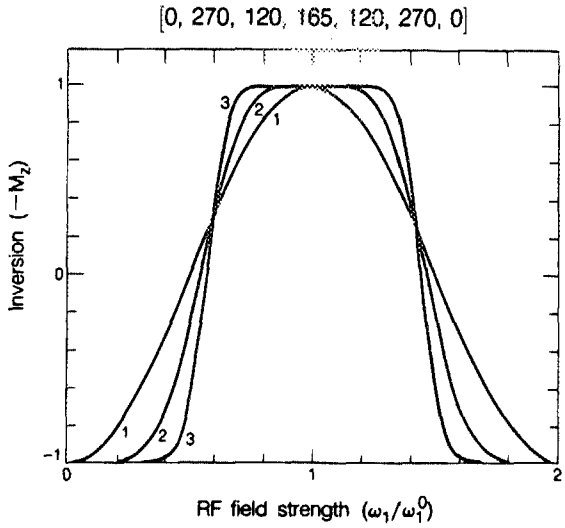

FIG. 10. Theoretical plots of population inversion as a function of normalized radiation amplitude for the (1) zeroth, (2) first, and (3) second iterations of the scheme [0, 270, 120, 165, 120, 270, 0]. The initial sequence S_0 is a single pulse with variable ω_1. The equilibrium polarization (magnetization aligned with the field) is denoted by -1, a complete inversion of the polarization by $+1$ (magnetization antiparallel to the field).

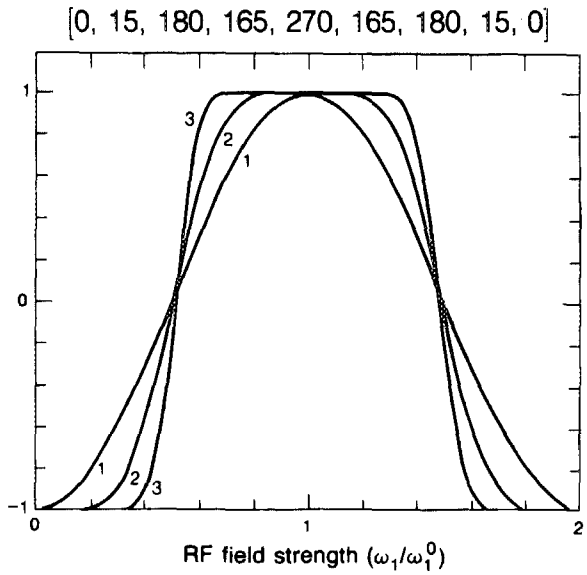

FIG. 11. Same as Fig. 10 but for the scheme [0, 15, 180, 165, 270, 165, 180, 15, 0].

pulse, and two iterations of the scheme. Two significant features of these plots stand out. First, it is clear that as the schemes are iterated, the bandwidth of the inversion response becomes increasingly more square. Within a sharply defined ω_1 range, the inversion achieved by the second iterate sequences is essentially complete. Outside this range, the rf has virtually no observable effect on the spins, leaving the bulk magnetization in its equilibrium state aligned with the static magnetic field.

The second notable characteristic of these plots are the two points in both where all three inversion curves intersect. The presence of these intersection points signifies an invariance in the inversion performance of these sequences for certain critical values of ω_1. These critical values are given by

$$\bar{\alpha}_{\text{unstable}} = \omega_1 t_p \bmod 2\pi, \tag{26a}$$

$$2\pi - \bar{\alpha}_{\text{unstable}} = \omega_1 t_p \bmod 2\pi \tag{26b}$$

providing indirect evidence of the unstable fixed point between the two stable points predicted earlier.

C. Role of the initial condition and some specific sequences

1. Single pulse initial condition

Experimental verification of the theoretical simulations for the first two iterates of both schemes appears in Figs. 12 and 13. The pulse sequence S_0 used to initiate the iterative

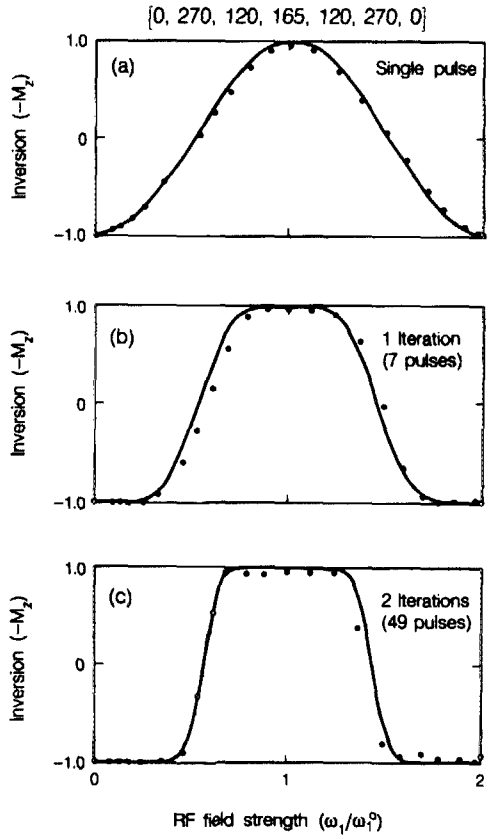

FIG. 12. Plot of population inversion as a function of radiation amplitude for the zeroth, first, and second iterations of the scheme [0, 270, 120, 165, 120, 270, 0]. The theoretical dependence appears as the black line, the experimental points as the dots.

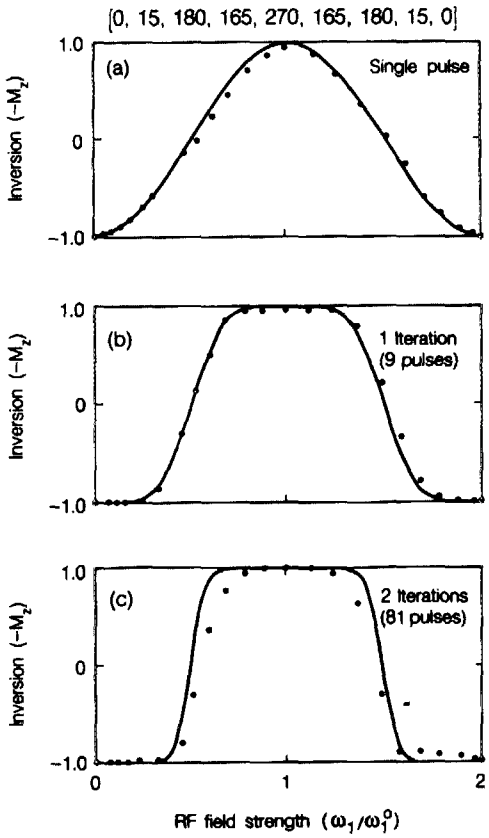

FIG. 13. Same as Fig. 12, but for the scheme [0, 15, 180, 165, 270, 165, 180, 15, 0].

procedure was a single pulse with variable ω_1. These results confirm the extreme specificity of these sequences for discriminating between spins based on the local rf field amplitude at the spin's coordinates in space.

The performance of these sequences off resonance is shown in Figs. 14 and 15. For single pulses, moving off resonance introduces a z component into the axis of rotation of the operator R. Due to the instability of the map at the origin along the z direction, the introduction of this z component in the initial iterate causes the bistability of the map to break down. As a result, the square response is irrevocably lost, even for the higher iterate sequences.

Although the useful bandpass specificity of these sequences is not retained off resonance, these plots nevertheless reveal an interesting fact. The nine shift sequence it may be recalled was derived to be stable in all directions at the equator. This additional stability, to some degree, compensates for off resonance effects near the equator. This compensation is indeed observed in these figures. Within the effective inversion range of the nine shift scheme, moving off resonance impairs inversion performance very little. For the seven shift sequence, however, the inversion performance is affected much more dramatically by going off resonance. This scheme, unlike the former scheme, does not produce stability at the equator, and hence is not compensated for resonance offset related imperfections.

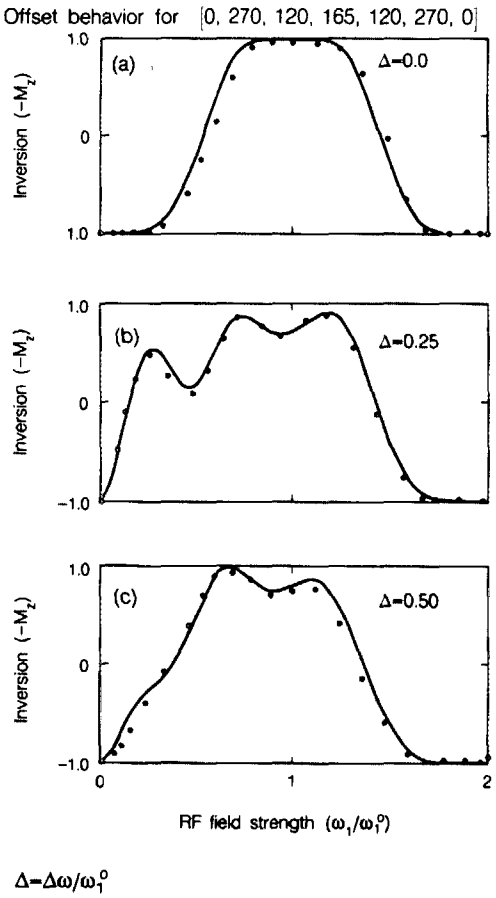

FIG. 14. Inversion performance of the scheme [0, 270, 120, 165, 120, 270, 0] at various resonance offsets. The sequence shown was generated by iterating once with this scheme on a single pulse of variable ω_1. Experimental points appear as the black dots.

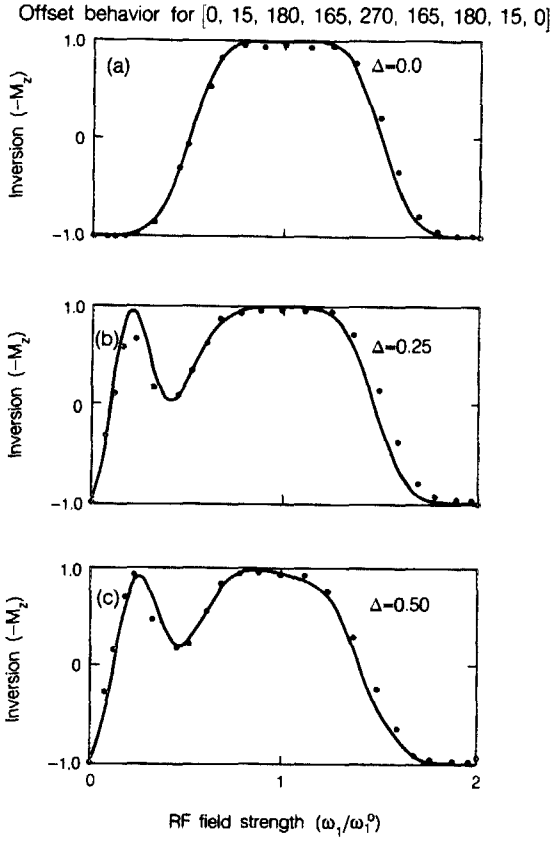

FIG. 15. Same as Fig. 14 but for the scheme [0, 15, 180, 165, 270, 165, 180, 15, 0].

2. Tailored inversion

The discussion of the previous sections has emphasized the fact that by varying experimental parameters, such as ω_1, of a starting sequence S_0, the coordinates in $SO(3)$ of the corresponding propagator $R(\alpha_0)$ can be varied in a well defined fashion as well. This can lead to interesting bandwidth behavior if, for example, for some values of ω_1, $R(\alpha_0)$ lies in the basin of one fixed set, and for other values of ω_1, $R(\alpha_0)$ lies in the basin of a second fixed set. Figure 16 illustrates this principle. Continuous variation of an experimental parameter λ causes $U_0(\lambda)$ to trace out a trajectory in Liouville space, taking it from the basin of one fixed set to the basin of another fixed point. This point was examined specifically for the case of an initial sequence S_0 consisting of a single resonant pulse and is manifested in the inversion vs ω_1 plots shown in Figs. 10 and 11, particularly for the higher iterate sequences. For values of ω_1 for which $R(\alpha_0)$ lies within the basin of the origin, the density operator remains unchanged from its initial state $-I_z$. Where ω_1 assumes values placing $R(\alpha_0)$ in the basin of the equator, however, nearly complete inversion of the density operator takes place.

The choice of a single pulse as the initial sequence resulted in a specific distribution of first iterates $R(\alpha_0)$ as a function of ω_1. If the phase of this pulse is 0°, this distribution of

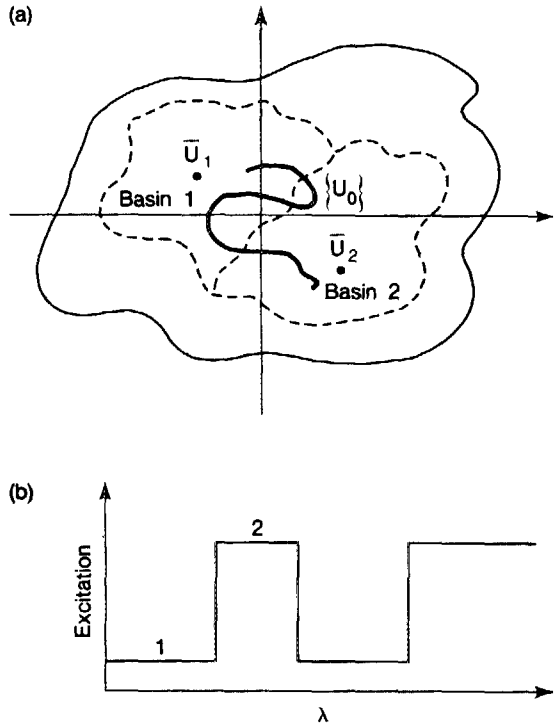

FIG. 16. Schematic illustration in (a) of a propagator U resulting from some excitation sequence plotted in propagator space as a function of some experimental parameter λ. The parametric dependence causes U to lie in the basin of one fixed point for some values of λ and in the basin of another fixed point for other values of λ, leading to the type of bandwidth behavior appearing in (b).

$R(\alpha_0)$ appears in $SO(3)$ as a continuous line from the origin to the equator along the x axis, as shown in Fig. 5(a). This distribution, along with the values of ω_1 for which $R(\alpha_0)$ crosses the unstable fixed circle, fully determines the bandwidth properties of the higher order iterates.

The variation of ω_1 can result in other, different distributions of $R(\alpha_0)$ simply if we choose a different S_0 as our starting sequence, for it is the specific form of S_0 which determines how $R(\alpha_0)$ varies as a function of ω_1. For values of ω_1 for which $R(\alpha_0)$ lies outside the unstable fixed circle, $R(\alpha_i)$ will converge to an inverting rotation as the map is iterated. Accordingly, over these ranges of ω_1, the density operator will be effectively inverted, particularly for the higher iterate sequences. For the remaining values of ω_1, $R(\alpha_0)$ will lie within the unstable fixed circle. Over these ranges of ω_1, $R(\alpha_0)$ converges to the identity operator as the map is iterated, resulting in sequences which do not alter the initial state of the spin system.

Generalizing this technique offers the possibility of a true tailoring of spin excitation. To achieve such tailoring, an initial sequence S_0 is chosen with the property that in the ranges of ω_1 for which population inversion is desired, $R(\alpha_0)$ lies within the basin of the equator. Iterating upon such an initial condition will then result in a pulse sequence which selectively and precisely inverts populations only over those regions of ω_1 for which $R(\alpha_0)$ lies within the proper basin. Although it is possible to obtain such starting sequences by analytical means, a more practical and equally effective approach would be to simply program a computer to search for sequences which fulfill the desired basin criteria.

3. Broadband and narrowband initial sequence

The rotation operators corresponding to inverting sequences broadband in ω_1 lie close to the equator of $SO(3)$ for a wide range of ω_1 values. Such sequences result in a distribution of initial rotations $R_\phi(\alpha_0)$ which lie predominantly within the basin of the equator for a bistable iterative scheme. Employing a broadband sequence as the initial iterate S_0 in a bistable iterative scheme therefore results in an inversion profile which becomes both square and broadband as the scheme is repeatedly applied.

The simulated inversion profiles appearing in Fig. 17 confirm this prediction. The sequence used in these plots to initiate the iterative procedure was the three pulse sequence [0, 120, 0], which has previously been shown to be effective in inverting spin populations over broad ranges of amplitudes.[11] Utilized as the initial iterate of the bistable iterative scheme, in this case the scheme [0, 270, 120, 165, 120, 270, 0], it produces the square, broadband inversion profile displayed in the higher iterates of Fig. 17.

A similar analysis is applicable to narrowband initial sequences as well. Within the theoretical picture presented here, narrowband sequences lead to distributions of rotation operators which, for most values of ω_1, lie close to the origin of $SO(3)$. For a very narrow range of ω_1 values, the rotation operators corresponding to the pulse sequence lie on the equator. Iterating on points distributed in such a way on $SO(3)$ results in a square, narrowband response.

Again, this can be confirmed by simulations of inversion performance, as shown in Fig. 18 for the initial narrowband sequence [0, 151, 255.5, 151, 0]. The inversion passband for

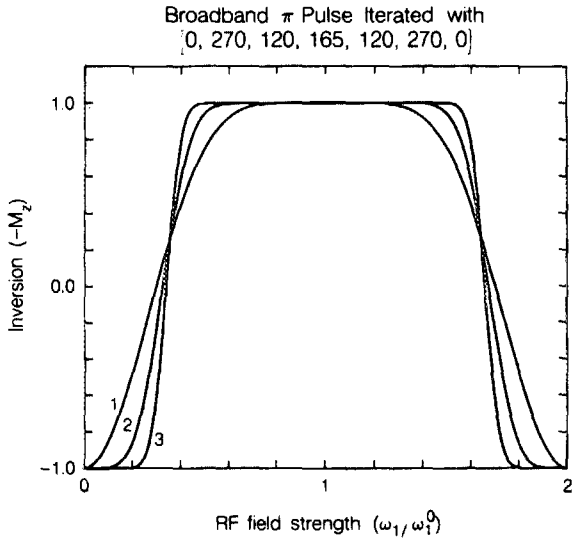

FIG. 17. Consequence of using a broadband sequence as the initial iterate for the bistable scheme [0, 270, 120, 165, 120, 270, 0] for the (1) zeroth, (2) first, and (3) second iteration of the scheme. The broadband sequence chosen here is the symmetric three pulse sequence [0, 120, 0].

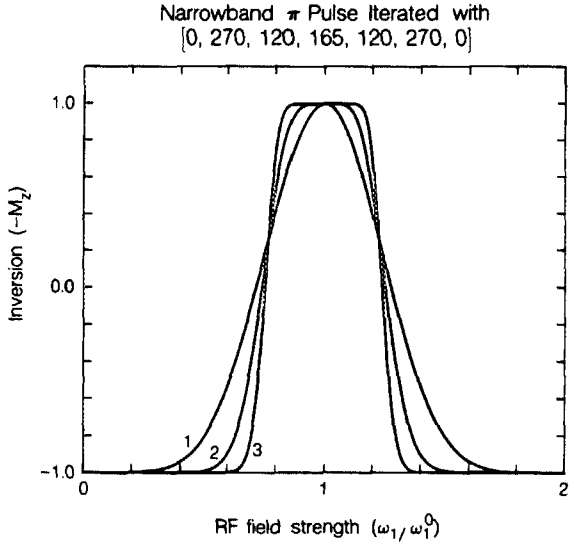

FIG. 18. Consequence of using a narrowband sequence as the initial iterate for the bistable scheme [0, 270, 120, 165, 120, 270, 0] for the (1) zeroth, (2) first, and (3) second iteration of the scheme. The narrowband sequence shown is the symmetric five pulse sequence [0, 151, 255.5, 151, 0].

higher iterates of this five pulse sequence is extremely narrow, reflecting the narrowband properties of the initial sequence.

We conclude by noting that both the narrowband and the broadband initial sequences display evidence of the unstable fixed point in the two crossing points delineating the effective passband of the two sequences, just as in the case of the single pulse initial condition.

4. Amplitude selective $\pi/2$ pulse sequences

The inversion vs ω_1 plots for the higher iterate pulse sequences obtained by the bistable maps reveals that the ω_1 ranges for which inversion of the density operator is complete and the ranges for which there is little inversion are separated by an extremely narrow range of ω_1 values where only partial inversion of the density operator takes place. As noted earlier, these narrow ranges indicate that at, or near these values of ω_1 the function $R(\alpha_0)$ crosses the unstable fixed circle.

Within this narrow range of ω_1 values lies an even narrower range where the projection of the density operator onto I_z is approximately zero after irradiation by the pulse sequence. This situation arises when the density operator has been rotated into the xy plane, and occurs when the overall propagator can be written:

$$U(t) = \exp[-i(\pi/2)(I_x \cos\phi + I_y \sin\phi)]. \quad (27)$$

The pulse sequences leading to such a propagator are known as $\pi/2$ sequences. In NMR terminology, the effect of the pulse sequence is to convert longitudinal polarization into transverse polarization.

The narrowness of the range of ω_1 values which result in such a propagator suggests a method for obtaining a highly amplitude selective $\pi/2$ pulse sequence. The ω_1 selectivity of such a sequence is limited only by the sharpness of the inversion bandpass cutoff, which, as has been demonstrated, can be made arbitrarily sharp by performing more operations of the iterative scheme. The creation of transverse magnetization only over narrow, specific ranges of ω_1 is an essential technique in applications such as slice-selective, *in vivo* NMR experiments,[32] which rely on rf amplitude gradients in order to preferentially excite selected regions of a macroscopic sample. The success of such an experiment depends on the ability to excite detectable NMR signal only in the regions of interest, and to suppress, or avoid excitation, of signal from other regions. In addition, it is desirable that the excitation sequence be short and consist only of pulses with the four quadrature phases.

The sequence $[(37.5)_{90}\ (37.5)_0\ (37.5)_{90}]$ was selected with these considerations in mind. The pulse sequence defined by this notation consists of three equal length pulses, each producing a flip angle of 37.5°, with phases 90°, 0°, 90°. In order to avoid exciting transverse signal at other values of ω_1 besides the intended range, the sequence picked is a broadband near-inverting sequence over ω_1 frequencies. Choosing such a sequence ensures that $R(\alpha_0)$ crosses the unstable fixed circle in the xy plane of $SO(3)$ only once over a large range of ω_1 values, in this case, the normalized range $0 \leqslant (\omega_1/\omega_1^0) \leqslant 8$. In this way, the creation of transverse magnetization in the higher iterate sequences at values of ω_1 other than the desired ones is suppressed. A more thorough examination of the problems associated with the inadvertent excitation of transverse coherence has been presented elsewhere.[64]

The ω_1 specificity obtainable from this method can be observed in Figs. 19 and 20 for this choice of an initial sequence. The top figures show the inversion plotted as a function of ω_1, while the lower figures show the projection of the density operator onto the xy plane after application of the pulse sequence. This last quantity is formally defined by the relation

$$\langle I_{xy} \rangle = (\{\mathrm{Tr}[I_x U(t) I_z U^\dagger(t)]\}^2 + \{\mathrm{Tr}[I_y U(t) I_z U^\dagger(t)]\}^2)^{1/2}/\mathrm{Tr}\{I_z^2\}. \quad (28)$$

Using this three pulse sequence as the starting point of the iterative procedure generates, after the nth iteration, sequences of length 3×7^n pulses for the seven shift scheme, and of length 3×9^n pulses for the nine shift scheme. These data verify the extreme specificity that can be obtained from using the cutoff frequency of a sharply defined ω_1 passband.

D. Experimental

The experiments described here were performed on a homebuilt spectrometer in a 4.2 T superconducting magnet. All experimental data were collected from the proton resonance of a distilled water sample sealed in a 1.5 mm diameter capillary tube.

Excitation sequences with nonquadrature phase shifts were generated at the intermediate frequency (30 MHz) by a Daico Industries 100D0898-30 8-bit digital phase shifter with 4 μs settling time and 360/256 deg phase resolution. An

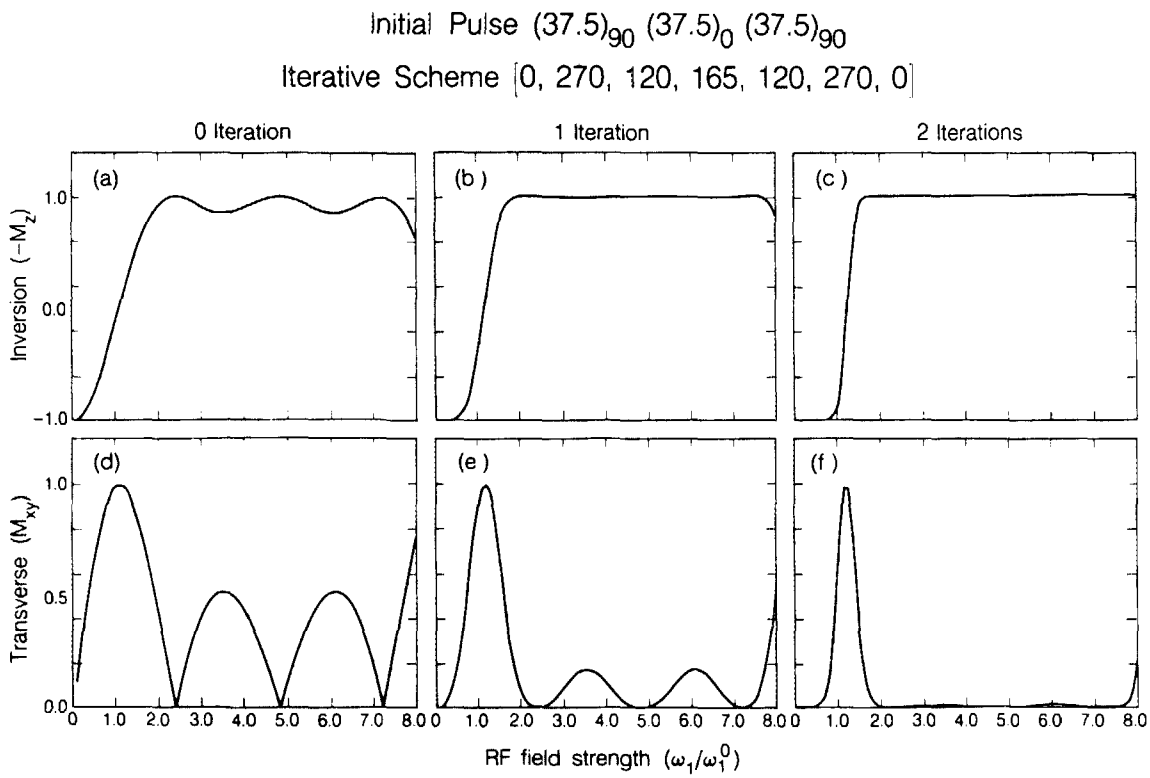

FIG. 19. Longitudinal [(a), (b), and (c)] and transverse [(d), (e), and (f)] magnetization plotted as functions of normalized radiation amplitude for the scheme [0, 270, 120, 165, 120, 270, 0] using the sequence $(37.5)_{90}$ $(37.5)_0$ $(37.5)_{90}$ as the zeroth iterate. The zeroth through second iterates are shown.

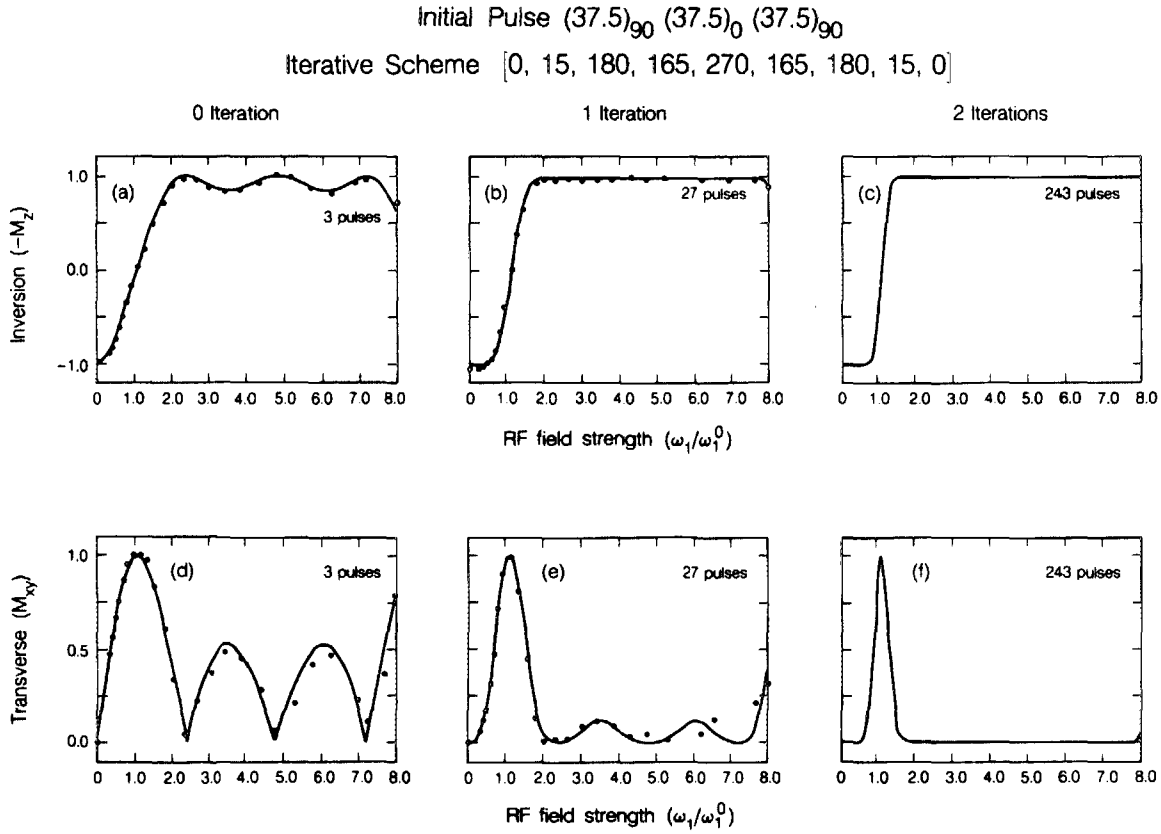

FIG. 20. Same as Fig. 21, but for the iterative scheme [0, 15, 180, 165, 270, 165, 180, 15, 0]. Where shown, experimental data appear as dots.

8×1024 programmable RAM was used to store the phase shift sequence for each experiment. The amplitudes and relative phases of the pulses were checked with a vector voltmeter to ensure their accuracy and uniformity.

The inversion performance of a pulse sequence was measured by following the inversion sequence with an appropriate dephasing delay, a $\pi/2$ on-resonance read pulse, and then acquisition of the free induction decay (FID). The dephasing delay was chosen to be long with respect to the inverse linewidth but short compared to the spin-lattice relaxation time. The linewidth of the proton resonance was inhomogeneously broadened with the magnet shims to permit this. The degree of inversion was obtained as a function of the peak height of the Fourier-transformed absorption buffer signal normalized to the peak height of the absorption signal following a single $\pi/2$ read pulse. When measurement of the transverse magnetization, rather than the longitudinal magnetization, was desired, the dephasing delay and $\pi/2$ read pulse were omitted before acquisition of the FID.

Measurements of inversion for different values of ω_1 were accomplished by fixing the pulse time and varying the power input to the linear rf transmitter with a variable attenuator. Amplitudes were calculated directly from the measured $\pi/2$ and π pulse times for each level of attenuation. Pulse times were found using standard calibration techniques.[65–67]

In order to determine the inversion performance of a pulse sequence off resonance, the radio frequencies for the pulse sequence and the read pulse were generated in separate rf channels and combined at the input to the rf transmitter, enabling the independent variation of the two irradiation frequencies. In this way, the excitation could be performed off resonance and the detection performed always on resonance.

V. OTHER ROUTES TO BISTABLE MAPS

In Sec. III, it was demonstrated that maps which were stable at the equator and the origin could be obtained by satisfying the stability conditions represented by Eqs. (22a) and (22b). Bistable maps can also be devised by forming composite maps out of two singularly stable maps, a topic which will be examined in the present section.

Consider two one dimensional maps F_1 and F_2 on the space L satisfying the relationships below:

$$F_1(\bar{x}_1) = \bar{x}_1, \tag{29a}$$

$$F_1(\bar{x}_2) = \bar{x}_2, \tag{29b}$$

$$\left|\frac{dF_1}{dx}\right|_{x=\bar{x}_1} < 1, \tag{29c}$$

$$\left|\frac{dF_1}{dx}\right|_{x=\bar{x}_2} > 1, \tag{29d}$$

$$F_2(\bar{x}_1) = \bar{x}_1, \tag{29e}$$

$$F_2(\bar{x}_2) = \bar{x}_2, \tag{29f}$$

$$\left|\frac{dF_2}{dx}\right|_{x=\bar{x}_1} > 1, \tag{29g}$$

$$\left|\frac{dF_2}{dx}\right|_{x=\bar{x}_2} < 1. \tag{29h}$$

Equations (29a), (29b), (29c), and (29f) indicate that F_1 and F_2 have the same two fixed points $\bar{x}_1$ and $\bar{x}_2$. By Eqs. (29c) and (29d) F_1 is stable at $\bar{x}_1$, but unstable at $\bar{x}_2$, while by Eqs. (29g) and (29h), F_2 is unstable at $\bar{x}_1$ but stable at $\bar{x}_2$.

We define the composition of these two maps by the following relation:

$$F_1 * F_2 = F_1[F_2(x)]. \tag{30}$$

It is clear that $F_1 * F_2$ will also be a map on L, with $\bar{x}_1$ and $\bar{x}_2$ both as fixed points.

The stability of $F_1 * F_2$ at $\bar{x}_1$ and $\bar{x}_2$ can be determined by evaluating the first derivative of $F_1 * F_2$ at the fixed points. By the chain rule, this derivative can be written:

$$\frac{d}{dx}(F_1 * F_2) = \frac{dF_1}{dF_2}\frac{dF_2}{dx}. \tag{31}$$

Using the general one dimensional stability criterion appearing in Eq. (3), the conditions for the stability of F_1 and F_2 at $\bar{x}_1$ and $\bar{x}_2$ can be stated as

$$\left|\frac{dF_2}{dx}\right|_{x=\bar{x}_1} < \left|\left[\frac{dF_1}{dF_2}\right]^{-1}\right|_{x=\bar{x}_1}, \tag{32a}$$

$$\left|\frac{dF_2}{dx}\right|_{x=\bar{x}_2} < \left|\left[\frac{dF_1}{dF_2}\right]^{-1}\right|_{x=\bar{x}_2}. \tag{32b}$$

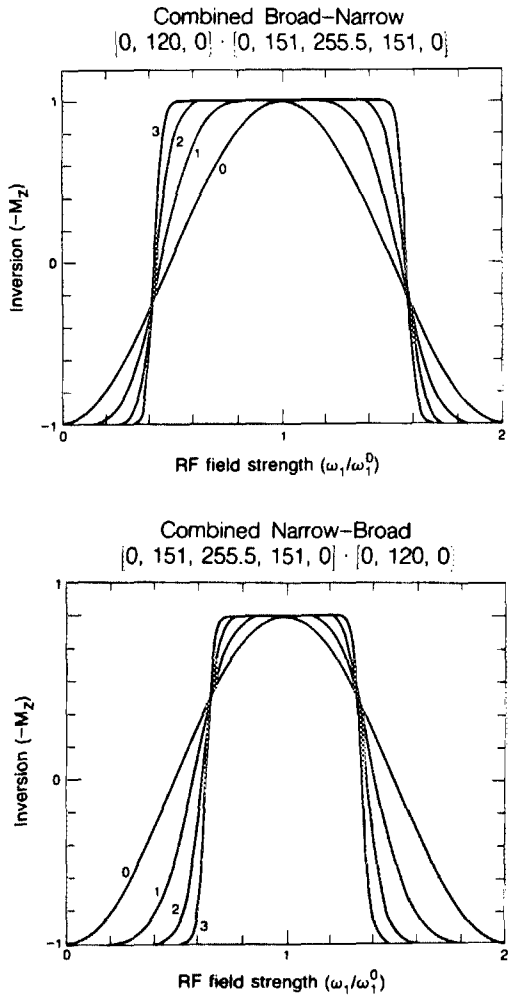

FIG. 21. Population inversion as a function of ω_1 for composite (broadband)*(narrowband) and (narrowband)*(broadband) schemes. The distinctive features of a bistable response are clearly evident in these profiles.

These inequalities are trivially satisfied if $\bar{x}_1$ is a superstable fixed point of F_1 and $\bar{x}_2$ a superstable fixed point of F_2 [provided the expression on the left-hand side of Eq. (32a) is finite]. Under these conditions, $\bar{x}_1$ and $\bar{x}_2$ will be stable fixed points of $F_1 * F_2$.

This result was used to devise a composite iteration scheme formed by alternating the broadband iterative scheme [0, 120, 0] with the narrowband iterative scheme [0, 151, 255.5, 151, 0]. These sequences were discussed in Sec. IV C. One iteration of the composite scheme on some sequence results in a sequence 15 times longer than the previous iterate. The symmetry of these schemes indicates that their corresponding maps will be single dimensional for initial iterates lying in the xy plane of $SO(3)$.

The composite scheme leads to a composite, one dimensional map on the xy plane of $SO(3)$ which is bistable, with all the attendant properties observed earlier for the two schemes (A) and (B). The inversion profiles bear this out, as can be seen in Fig. 21. Although the width of the passband is dependent upon the order of the composition, both still display the distinctive bandpass features seen before indicative of the underlying bistable map.

ACKNOWLEDGMENTS

We are grateful to R. Tycko and J. Guckenheimer for many helpful discussions. D. Shykind provided expert technical assistance. J. B. held a University of California President's Fellowship. This work was supported by the Director, Office of Energy Research, Office of Basic Energy Sciences, Materials Sciences Division of the U.S. Department of Energy under Contract No. DE-AC03-76SF00098.

[1] A. G. Redfield, S. D. Kunz, and E. K. Ralph, J. Magn. Reson. **19**, 114 (1975).
[2] M. H. Levitt and R. Freeman, J. Magn. Reson. **33**, 473 (1979).
[3] R. Freeman, S. P. Kempsell, and M. H. Levitt, J. Magn. Reson. **38**, 453 (1980).
[4] M. H. Levitt and R. Freeman, J. Magn. Reson. **43**, 65 (1981).
[5] M. H. Levitt, J. Magn. Reson. **48**, 234 (1982).
[6] M. H. Levitt, J. Magn. Reson. **50**, 95 (1982).
[7] R. Tycko, Phys. Rev. Lett. **51**, 775 (1983).
[8] J. Baum, R. Tycko, and A. Pines, J. Chem. Phys. **79**, 4643 (1983).
[9] M. H. Levitt and R. R. Ernst, J. Magn. Reson. **55**, 247 (1983).
[10] A. J. Shaka and R. Freeman, J. Magn. Reson. **55**, 487 (1983).
[11] R. Tycko and A. Pines, Chem. Phys. Lett. **111**, 462 (1984).
[12] R. Tycko, H. M. Cho, E. Schneider, and A. Pines, J. Magn. Reson. **61**, 90 (1985).
[13] J. Baum, R. Tycko, and A. Pines, Phys. Rev. A **32**, 3435 (1985).
[14] R. Tycko, A. Pines, and J. Guckenheimer, J. Chem. Phys. **83**, 2775 (1985).
[15] M. H. Levitt, Prog. Nucl. Magn. Reson. Spectrosc. **18**, 61 (1986).
[16] A. J. Shaka and R. Freeman, J. Magn. Reson. **59**, 169 (1984).
[17] M. H. Levitt and R. Freeman, J. Magn. Reson. **43**, 502 (1981).
[18] M. H. Levitt, R. Freeman, and T. Frenkiel, J. Magn. Reson. **47**, 328 (1982).
[19] J. S. Waugh, J. Magn. Reson. **49**, 517 (1982).
[20] M. H. Levitt, R. Freeman, and T. Frenkiel, J. Magn. Reson. **50**, 157 (1982).
[21] J. S. Waugh, J. Magn. Reson. **50**, 30 (1982).
[22] A. J. Shaka, J. Keeler, T. Frenkiel, and R. Freeman, J. Magn. Reson. **52**, 335 (1983).
[23] A. J. Shaka, J. Keeler, and R. Freeman, J. Magn. Reson. **53**, 313 (1983).
[24] M. H. Levitt, R. Freeman, and T. Frenkiel, in *Advances in Magnetic Resonance*, edited by J. S. Waugh (Academic, New York, 1983), Vol. II.
[25] A. J. Shaka and J. Keeler, Prog. Nucl. Magn. Reson. Spectrosc. **19**, 47 (1986).
[26] T. M. Barbara, R. Tycko, and D. P. Weitekamp, J. Magn. Reson. **62**, 54 (1985).
[27] M. H. Levitt, D. Suter, and R. R. Ernst, J. Chem. Phys. **80**, 3064 (1984).
[28] R. Tycko, E. Schneider, and A. Pines, J. Chem. Phys. **81**, 680 (1984).
[29] M. H. Levitt and R. R. Ernst, Mol. Phys. **50**, 1109 (1983).
[30] J. R. Garbow, D. P. Weitekamp, and A. Pines, Chem. Phys. Lett. **93**, 504 (1982).
[31] H. M. Cho, R. Tycko, A. Pines, and J. Guckenheimer, Phys. Rev. Lett. **56**, 1905 (1986).
[32] J. J. H. Ackerman, T. H. Grove, G. G. Wong, D. G. Gadian, and G. K. Radda, Nature **283**, 167 (1980).
[33] (a) D. P. Weitekamp, A. Bielecki, D. Zax, K. Zilm, and A. Pines, Phys. Rev. Lett. **50**, 1807 (1983); (b) D. B. Zax, A. Bielecki, K. W. Zilm, A. Pines, and D. P. Weitekamp, J. Chem. Phys. **83**, 4877 (1985).
[34] W. S. Warren, S. Sinton, D. P. Weitekamp, and A. Pines, Phys. Rev. Lett. **43**, 1791 (1979).
[35] D. P. Weitekamp, in *Advances in Magnetic Resonance*, edited by J. S. Waugh (Academic, New York, 1983), Vol. 11.
[36] M. Munowitz and A. Pines, in *Advances in Chemical Physics*, edited by S. Rice and I. Prigogine (Wiley–Interscience, New York, 1986), Vol. 11.
[37] (a) G. Castro, D. Haarer, R. M. Macfarlane, and H. P. Trommsdorff, Frequency Selective Optical Data Storage System, U.S. Patent No. 4101976 (1978); (b) G. C. Bjorklund, W. Lenth, and C. Ortiz, Proc. Soc. Photo-Opt. Instrum. Eng. **298**, 107 (1981).
[38] U. Haeberlen and J. S. Waugh, Phys. Rev. **175**, 453 (1968).
[39] U. Haeberlen, *High Resolution NMR in Solids: Selective Averaging* (Academic, New York, 1976).
[40] M. Mehring, *Principles of High Resolution NMR in Solids*, 2nd ed. (Springer, New York, 1983).
[41] G. A. Morris and R. Freeman, J. Magn. Reson. **29**, 433 (1978).
[42] D. L. Turner, J. Magn. Reson. **54**, 146 (1983).
[43] P. J. Hore, J. Magn. Reson. **54**, 539 (1983).
[44] P. J. Hore, J. Magn. Reson. **55**, 283 (1983).
[45] M. S. Silver, R. I. Joseph, and D. I. Hoult, J. Magn. Reson. **59**, 347 (1984).
[46] A. Hasenfeld, Magn. Reson. Med. **2**, 505 (1985).
[47] F. A. Grunbaum, Inverse Problems **1**, L25 (1985).
[48] W. Magnus, Common Pure Appl. Math. **7**, 649 (1954).
[49] F. Bloch, Phys. Rev. **70**, 460 (1946).
[50] W. S. Warren, D. P. Weitekamp, and A. Pines, J. Chem. Phys. **73**, 2084 (1980).
[51] R. M. May, Nature **261**, 459 (1976).
[52] *Nonlinear Dynamics*, edited by R. H. G. Helleman (New York Academy of Sciences, 1980), p. 357.
[53] M. J. Feigenbaum, Physica (Amsterdam) D **7**, 16 (1983).
[54] M. W. Hirsch and S. Smale, *Differential Equations, Dynamical Systems and Linear Algebra* (Academic, New York, 1974).
[55] I. Percival and D. Richards, *Introduction to Dynamics* (Cambridge University, Cambridge, 1982).
[56] P. Collet and J. P. Eckmann, *Iterated Maps on the Interval as Dynamical Systems* (Birkhauser, Boston, 1980).
[57] J. Guckenheimer and P. Holmes, *Nonlinear Oscillations, Dynamical Systems, and Bifurcations of Vector Fields* (Springer, New York, 1983).
[58] R. P. Feynman, F. L. Vernon, and R. W. Hellwarth, J. Appl. Phys. **28**, 49 (1957).
[59] For a two level system, the operator $U(t)$ in Eq. (6) can be written in matrix form as a 2×2 unitary matrix with determinant equal to one. The set of all such matrices forms the group $SU(2)$. In what follows, however, we shall regard $U(t)$ as an element of the real three dimensional rotation group $SO(3)$, which is related to $SU(2)$ by a twofold homomorphism. Except for immaterial phase factors, the differences between these two groups can, for all practical purposes, be ignored. Accordingly, we shall consider all propagators of the form given by Eq. (6) as being essentially equivalent to three dimensional rotations.
[60] H. Goldstein, *Classical Mechanics*, 2nd ed. (Addison–Wesley, Reading, Mass., 1980).
[61] M. I. Petrashen and E. D. Trifonov, *Applications of Group Theory in*

Quantum Mechanics (M.I.T., Cambridge, Mass., 1969).
[62]L. W. Johnson and R. D. Riess, *Numerical Analysis* (Addison–Wesley, Reading, Mass., 1977).
[63]B. Mandelbrot, *Fractals: Form, Chance, and Dimension* (Freeman, San Francisco, 1977).
[64]J. Baum, R. Tycko, and A. Pines, Chem. Phys. **105**, 7 (1986).
[65]P. Mansfield, M. J. Orchard, D. C. Stalker, and K. H. B. Richards, Phys. Rev. B 7, 90 (1973).
[66]R. W. Vaughn, D. D. Elleman, L. M. Stacey, W. K. Rhim, and J. W. Lee, Rev. Sci. Instrum. **43**, 1356 (1972).
[67]W. K. Rhim, D. D. Elleman, L. B. Schreiber, and R. W. Vaughn, J. Chem. Phys. **60**, 4595 (1974).